Geological Magazine

www.cambridge.org/geo

Tectonic differentiation and thermal history of the eastern Ordos Basin (central-western China) since the Mesozoic

Sasa Guo[1,2], Zhanli Ren[1,2], Andrew C. Kerr[3], Kai Qi[1,2], Guangyuan Xing[1,2], Liyong Fan[4] and Jinbu Li[4]

[1]Department of Geology, Northwest University, Xi'an, China; [2]State Key Laboratory of Continental Evolution and Early Life, Northwest University, Xi'an, China; [3]School of Earth and Environmental Sciences, Cardiff University, UK and [4]Exploration and Development Research Institute of PetroChina Changqing Oilfield, Xi'an, China

Original Article

Cite this article: Guo S, Ren Z, Kerr AC, Qi K, Xing G, Fan L, and Li J. Tectonic differentiation and thermal history of the eastern Ordos Basin (central-western China) since the Mesozoic. *Geological Magazine* **163**(e13): 1–15. https://doi.org/10.1017/S0016756826100545

Received: 9 July 2025
Revised: 7 January 2026
Accepted: 8 January 2026

Keywords:
Ordos Basin; apatite fission track; thermal history; low-temperature thermochronology; thermal evolution

Corresponding author:
Zhanli Ren; Email: renzhanl@nwu.edu.cn

Abstract

The eastern Ordos Basin is situated in a transitional zone between the stable Ordos craton and an adjacent active orogenic belt. Episodic tectonic uplift and subsequent cooling of the eastern Ordos Basin since the Mesozoic have been spatially and temporally heterogeneous, with uplift and cooling commencing earlier in the central and northern segments than in the south. To constrain the differential tectono-thermal history of the eastern region, apatite fission-track analyses were carried out on Upper Palaeozoic samples from distinct tectonic units, and new data are presented. The results identify four discrete episodes of rapid exhumation at 110 Ma, 70 Ma, 50 Ma, and 30 Ma, confirming a heterogeneous uplift and exhumation history of the region since the Early Cretaceous. The Eastern Ordos has experienced three phases of uplift. North-south thermal histories differ significantly: the south shows later, rapid cooling (50 m/Ma, 110–90 Ma), while the north shows earlier, slower exhumation (25 m/Ma, 130–90 Ma). Since 30 Ma, the southern area experienced accelerated uplift, contrasting with the moderate exhumation observed in the north and centre. We infer that differential tectonic uplift, exhumation, and the cooling process are coupled to underlying mantle dynamics, which have resulted in the complex structure of the eastern basin. This research provides significant implications for reconstructing the divergent thermal evolution pathways of its various tectonic units.

1. Introduction

The Ordos Basin is a major cratonic sedimentary basin in central-western China, which hosts prolific hydrocarbon resources, and its tectonic evolution has significantly influenced the development of petroleum systems in the basin (Yang *et al.* 2024; Ju *et al.* 2025). The eastern margin of the basin is located within the Trans-North China Orogen (TNCO), a transitional zone between the strongly reactivated eastern North China Craton (NCC) and the relatively stable western NCC. Structurally, the TNCO is dominated by several major fault systems, including the Taihangshan Fault, Lvliangshan Fault, and the Fenhe–Weihe rift system. These fault systems exhibit two principal orientations, NNE–SSW and NW–SE, reflecting the stress regime associated with palaeo-orogenic tectonics (Li *et al.* 2021; Zhang *et al.* 2021*b*). As a result, the eastern margin of the Ordos Basin has undergone multiple tectonic and thermal events. The thermal history also exhibits significant spatial heterogeneity due to the tectonic interplay with adjacent units such as the Taihang and Lvliang Mountains, and the marginal tectonic belt of the NCC. Therefore, constraining the detailed tectonic activity in this region since the Mesozoic is not only helpful for understanding oil and gas distribution within the basin but will also provide crucial insights into the large-scale deformation that has shaped the entire eastern NCC since the Mesozoic.

A substantial body of work using a range of thermochronometers, such as zircon U-Pb, fission-track, and (U-Th)/He dating (Chen *et al.* 2007; Chen *et al.* 2013; Ren *et al.* 2015; Huang *et al.* 2016; Peng *et al.* 2019; Huang *et al.* 2021; Zhang *et al.* 2021*a*; Peng *et al.* 2022; Ren *et al.* 2022; Xu *et al.* 2022; He *et al.* 2023; Peng *et al.* 2023; Yang *et al.* 2023; Chen *et al.* 2025; Qi *et al.* 2025), has constrained the tectono-thermal evolution of the Ordos Basin and its eastern margin since the Mesozoic. This previous research has presented evidence that the eastern Ordos Basin and the Taihang-Lüliang Mountains have undergone at least four episodes of rapid exhumation since the Mesozoic (Ding *et al.* 2016; Huang *et al.* 2021; Zhang *et al.* 2021a; Chen *et al.* 2022; Chen *et al.* 2025). Furthermore, the shortening and deformation of the Taihang-Lvliang Mountains are most likely linked to the tectonic activity of the Palaeo-Pacific Plate (Clinkscales *et al.* 2021). These studies have also clarified the tectonic setting for the formation of the eastern margin of the basin and have provided constraints on its multi-stage exhumation from the Late Cretaceous to Cenozoic. Despite this previous work, systematic thermochronological research

across the entire eastern Ordos Basin remains limited, as these studies largely concentrated on the northeastern and southeastern corners of the basin or within the adjacent Lvliang Mountains. As a result, there remains a gap in our understanding of the differential uplift and cooling processes across the entire region. Consequently, the differences in cooling history between the various tectonic units of the eastern Ordos Basin and their underlying geodynamic mechanisms have not yet been fully resolved. This study addresses this gap by presenting new apatite fission-track (AFT) data from multiple transects across the eastern Ordos Basin. By integrating these data with the regional geological context, we can more precisely constrain the variations in tectonic activity and cooling processes of the different structural units. This work aims to provide new thermochronological constraints for reconstructing the tectonic evolution of the eastern Ordos Basin, while also offering crucial data for research into the tectono-thermal coupling at the margin of the NCC.

2. Geological setting

2.a. Tectonic background of the eastern Ordos Basin

The NW-SE trending Ordos Basin (Figure 1a) constitutes a major, long-term tectonically stable block within the NCC and is rich in hydrocarbon resources (Yang *et al.* 2023, 2024). Its eastern margin, however, is a tectonically active zone situated adjacent to the Lvliangshan structural belt, which is characterized by multi-stage, superimposed faulting and uplift events (Li *et al.* 2013, 2015; Ding *et al.* 2016). This eastern boundary is structurally defined by the Lvliang Mountains and is influenced by a tectonic deformation zone at the edge of the ancient North China block (Figure 1b and c). This deformation zone has resulted in multiple sets of NE–NNE trending fault systems (Zhang *et al.* 2021a). Compared to the Yishan Slope in the west, the stratigraphic thickness along the eastern margin of the basin is significantly reduced. The Lvliang Mountains exhibit significant north-south geological variations. The northern section is dominated by exposures of Carboniferous, Permian, Triassic, and Jurassic strata, whereas the southern section primarily consists of Carboniferous-Permian strata and Cambrian-Ordovician limestones, where a series of west-verging thrust faults has also developed (Zhang *et al.* 2021a). The basement of the Lvliangshan anticlines primarily consists of Palaeoproterozoic metamorphic rocks and Neoarchean to Palaeoproterozoic granites (Geng *et al.* 2000; Zhao *et al.* 2005). The denudation of the overlying strata varies; the northern area (Shenmu-Fugu) retains Jurassic strata, whereas the southern area is dominated by Cambrian-Ordovician and Carboniferous-Permian strata, accompanied by the development of a series of west-verging thrust faults (Zhang *et al.* 2021a). The structural pattern in the northern area is relatively simple, being characterized predominantly by NW-SE-trending normal faults. Further south, near Xingxian, these structures gradually evolve into an anticline, with fault types changing from normal to reverse. The central area, near Linxian, represents the zone of most intense tectonic deformation. Owing to the intrusion of the Zijinshan igneous, the overall structure exhibits a dome-shaped geometry. The strata on both limbs of the anticline are gently dipping and nearly horizontal, indicating a symmetrical fold. In the southern area, the faults transition into normal faults, arranged along the boundary between the Ordovician and Carboniferous strata. Further south, the structures are mainly characterized by synclines.

Since the Late Triassic, the Lvliangshan area has transitioned from a depocenter to a zone of denudation, showing a trend of continuous uplift (Zhang *et al.* 2021*a*). This uplift was especially rapid during the Early Cretaceous (ca. 150–100 Ma), when the region was subjected to intense compression at the margin of the NCC. During this compression, the region underwent significant structural inversion, leading to asymmetric uplift and denudation in the surrounding areas. The Cenozoic tectonic activity further intensified tectonic denudation and created distinct differences in cooling and thermal evolution pathways between the northern and southern parts of the region. Consequently, due to its unique location and structural characteristics, the Lvliangshan uplift has become a key tectonic element governing the thermal evolution of the eastern Ordos Basin.

3. Methods and data

3.a. Sampling and location selection

For this study, a total of 15 Upper Palaeozoic sandstone samples were collected from across the Lvliangshan uplift on the eastern margin of the Ordos Basin. The sample set comprises two Permian drill core samples from the Daji area and thirteen surface outcrop samples. These samples were systematically collected from Carboniferous, Permian, and Triassic strata, with sandstone being specifically targeted to ensure a sufficient yield of apatite crystals for analysis. The specific locations of all sampling sites are shown in Figures 1 and 2.

3.b. Fission-track analysis and age calculation

In this study, AFT analysis was carried out on 15 samples from the eastern Ordos Basin. For each sample, between 14 and 29 apatite grains were analysed. A minimum of three Dpar values were measured for each grain to characterize its annealing properties (Ketcham *et al.* 1999). Apatite grains were separated from the samples through standard crushing, magnetic, and heavy-liquid separation techniques by Yu-Neng Technology Service Limited Company, Langfang, Hebei, China. To reveal the fission tracks, the grains were etched with 5.5 Mol HNO_3 for 20 seconds at room temperature (Donelick *et al.* 2005).

Spontaneous fission-track counting and length measurements were performed using an automated microscopy system. The ^{238}U content of each grain was subsequently measured by LA-ICP-MS. Single-grain ages were calculated from the spontaneous track density and the measured U-concentration (Hasebe *et al.* 2013).

3.c. Thermal history modelling

Thermal history modelling was conducted using the HeFTy software (Ketcham, 2005), which employs a time-temperature box modelling approach. Key input parameters for the models included the AFT ages and the confined track-length distributions (with c-axis projection) within the Partial Annealing Zone (PAZ, 60–120°C). Known geological constraints, such as stratigraphic depositional ages and major exhumation events, were also incorporated. A present-day surface temperature of 20 ± 5°C was set for all modelled samples. To identify distinct uplift and cooling pathways controlled by the Lvliangshan uplift, separate initial models were established for samples from the northern and southern areas of the eastern basin.

https://doi.org/10.1017/S0016756826100545 Published online by Cambridge University Press

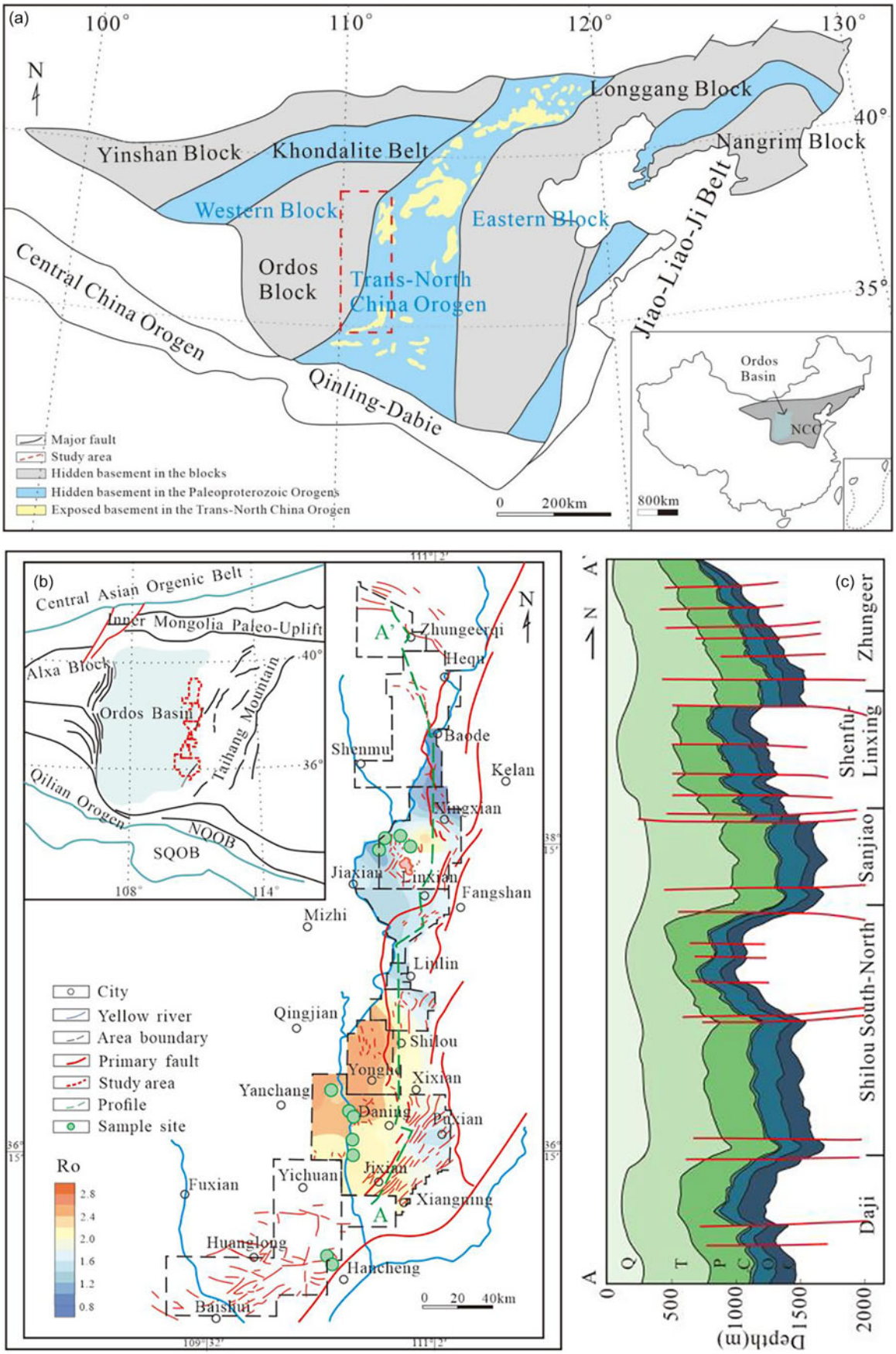

Figure 1. (a) Tectonic subdivision of the North China Craton (modified after Zhao et al. (2005)), (b) Structural location and thermal maturity distribution of Upper Palaeozoic strata (c) typical cross-section of eastern Ordos Basin, A-A' is the north-south cross-section, extending from Baode in the north to the Daji area in the south.

https://doi.org/10.1017/S0016756826100545 Published online by Cambridge University Press

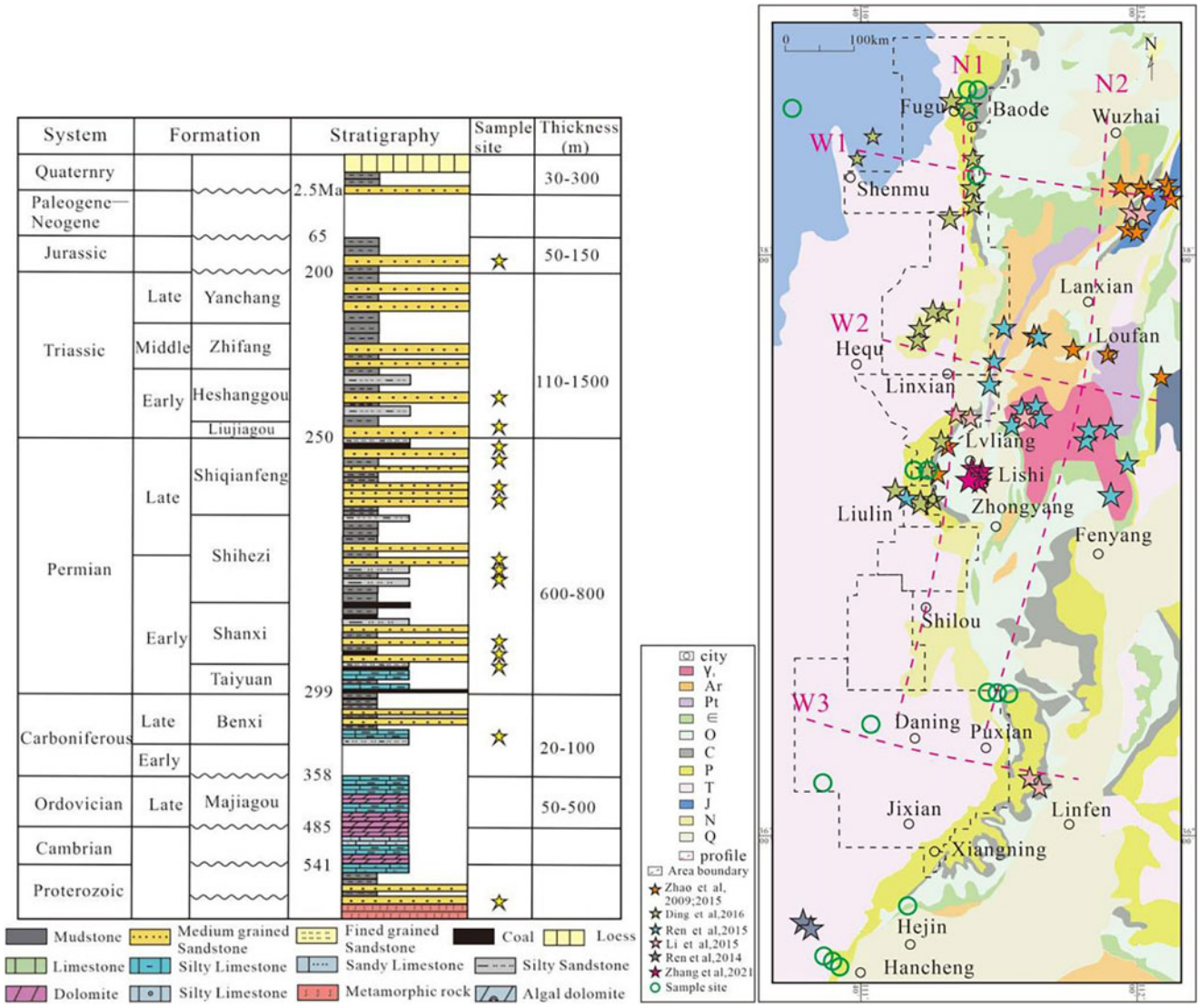

Figure 2. Stratigraphic column and distribution map of AFT sample locations (tectonic location is the same as in Figure 1b.) from the Eastern Ordos Basin.

4. Results

4.a. Fission-track results

Central ages, calculated using the RadialPlotter software (Vermeesch, 2008), range from 21.7 ± 4 Ma to 149.8 ± 18 Ma (Table 1). All samples failed the chi-squared (χ^2) test ($P(\chi^2) < 5\%$), indicating significant dispersion among their single-grain ages (Figure 3). Among the samples, one (XAK-8) is an intrusive igneous rock from the southeastern part of the basin, yielding an AFT age of 52.7 ± 6 Ma. A clear spatial trend is observed in the ages, with samples from the northeast being older (average AFT age: 124.8 Ma; oldest age: 149.8 ± 18 Ma) than those from the southeast (average AFT age: 53.9 Ma). The measured Dpar values range from 1.15 to 1.8 μm, extending beyond the typical range of the Durango apatite standard (1.5–1.9 μm; McDowell *et al.* 2005). This suggests that the apatite grains are compositionally diverse and possess variable annealing kinetics (Donelick *et al.* 2005). Furthermore, the single-grain age histograms typically exhibit bimodal distributions, indicating the influence of multiple thermal events. All samples' AFT ages are younger than their stratigraphic depositional ages. Their mean track lengths range from 11.5 ± 1.8 μm to 12.3 ± 1.8 μm, and are also significantly shorter than the initial length of ~16.3 μm (Gleadow *et al.* 1986). Therefore, all samples have experienced significant fission-track annealing, confirming that their AFT data are suitable for constraining the tectono-thermal history of the basin.

4.b. Reconstruction of uplift history

Thermal history modelling was carried out on individual samples using the HeFTy software (Ketcham, 2005), applying the annealing model of Ketcham (2007) and utilizes a Monte Carlo inversion algorithm. The initial conditions for the modelling were constrained by both fission-track data and the stratigraphic age. The exhumation of the eastern margin since the Mesozoic commenced in the Middle Jurassic (Zhang *et al.* 2021a) and potentially includes three cooling stages: the late Jurassic, Late Cretaceous, and early Cenozoic. To obtain a more reliable thermal history path during modelling (Figure 4), constraint boxes were set for the T-t (temperature-time) simulations based on potential cooling events since the Mesozoic. The modelling timeframe spans from the late Jurassic to the present (160–0Ma), with an initial temperature

https://doi.org/10.1017/S0016756826100545 Published online by Cambridge University Press

Table 1. New apatite fission-track data from Eastern Ordos Basin

Location	No.	Lithology	Strata	GPS	Estimated strata age	Elevation (m)	NG	Ns	ρs(×10^5/cm^2)	P(χ)(%)	U(ppm)	Pooled age (Ma ± 1σ)	Central age (Ma ± 1σ)	L(μm)(NL)
North	SM-3	Sandstone	J	110°10′42″E 39°3′13″N	170	1197	23	406	8.73	0	17.89	97.1 ± 18.6	107.8 ± 17.8	12.28 ± 1.8(51)
	HZM-1	Sandstone	P_1t	111°7′32″E 39°6′0″N	295	985	20	1037	10.1	0	15.89	130.9 ± 19.5	149.8 ± 18.4	10.48 ± 1.1(46)
	HZM-2	Sandstone	P_3s	111°7′32″E 39°6′0″N	260	987	20	1013	11.7	0	21.07	120.2 ± 11.5	127.0 ± 10.5	11.59 ± 1.6(71)
	HZM-7	Sandstone	P_1s	111°5′28″E 39°2′9″N	290	829	25	1169	10.1	0	25.44	80.2 ± 13.0	94.4 ± 10.9	13.7 ± 1.5(44)
	BD-13	Sandstone	C_2b	111°8′11″E 38°45′30″N	310	1052	14	410	13	0	18.22	111.6 ± 22.4	144.8 ± 18.7	11.1 ± 1.7(48)
Middle	CJZ-6	Sandstone	P_3s	110°49′57″E 37°32′56″N	260	781	25	738	6.78	0	22.58	59.3 ± 13.4	78.7 ± 9.7	11.53 ± 1.8(44)
	CJZ-8	Sandstone	P_1s	110°52′59″E 37°33′27″N	290	871.5	23	801	6.83	0	24.15	50.0 ± 11.6	68.5 ± 9.1	11.73 ± 1.9(52)
South	AZC-1	Sandstone	T	111°6′49″E 36°37′46″N	240	1056	25	812	11.5	0	59.35	39.2 ± 4.9	44.8 ± 4.5	10.3 ± 1.2(37)
	AZC-3	Sandstone	P	111°8′32″E 36°37′53″N	260	1090	25	1118	12.1	0	24.43	102.2 ± 14.2	111.2 ± 11.0	10.2 ± 1.6(45)
	ZYC-2	Sandstone	P_2s	110°22′27″E 35°29′53″N	265	458	22	654	11.2	0	33.03	53.9 ± 13.9	73.1 ± 10.3	–
	ZYC-4	Sandstone	P_3s	110°19′33″E 35°31′13″N	255	540	22	598	8.8	0	51.03	33.9 ± 12.1	46.3 ± 47.1	–
	ZYC-6	Sandstone	T_1l	110°18′3″E 35°32′10″N	250	630	23	727	10.4	0	50.35	42.2 ± 30.4	55.9 ± 10	11.87 ± 1(50)
	G3	Sandstone	P_1s	110°13’49’E 36°15’52’N	293		29	1291	5.47	0	43.43	25.4 ± 3.0	28.4 ± 2.3	–
	DJ21	Sandstone	P_3s	110°27’28’E 36°30’30’N	255		15	380	5.51	0	42.77	25.3 ± 5.4	27.1 ± 4.0	12.17 ± 1.7(45)
	XAK-8	Igneous	Pr	110°42′52″E 35°43′44″N	610	577	14	410	13.2	0	18.22	48.3 ± 3.1	52.7 ± 6.2	11.3 ± 1.7(52)

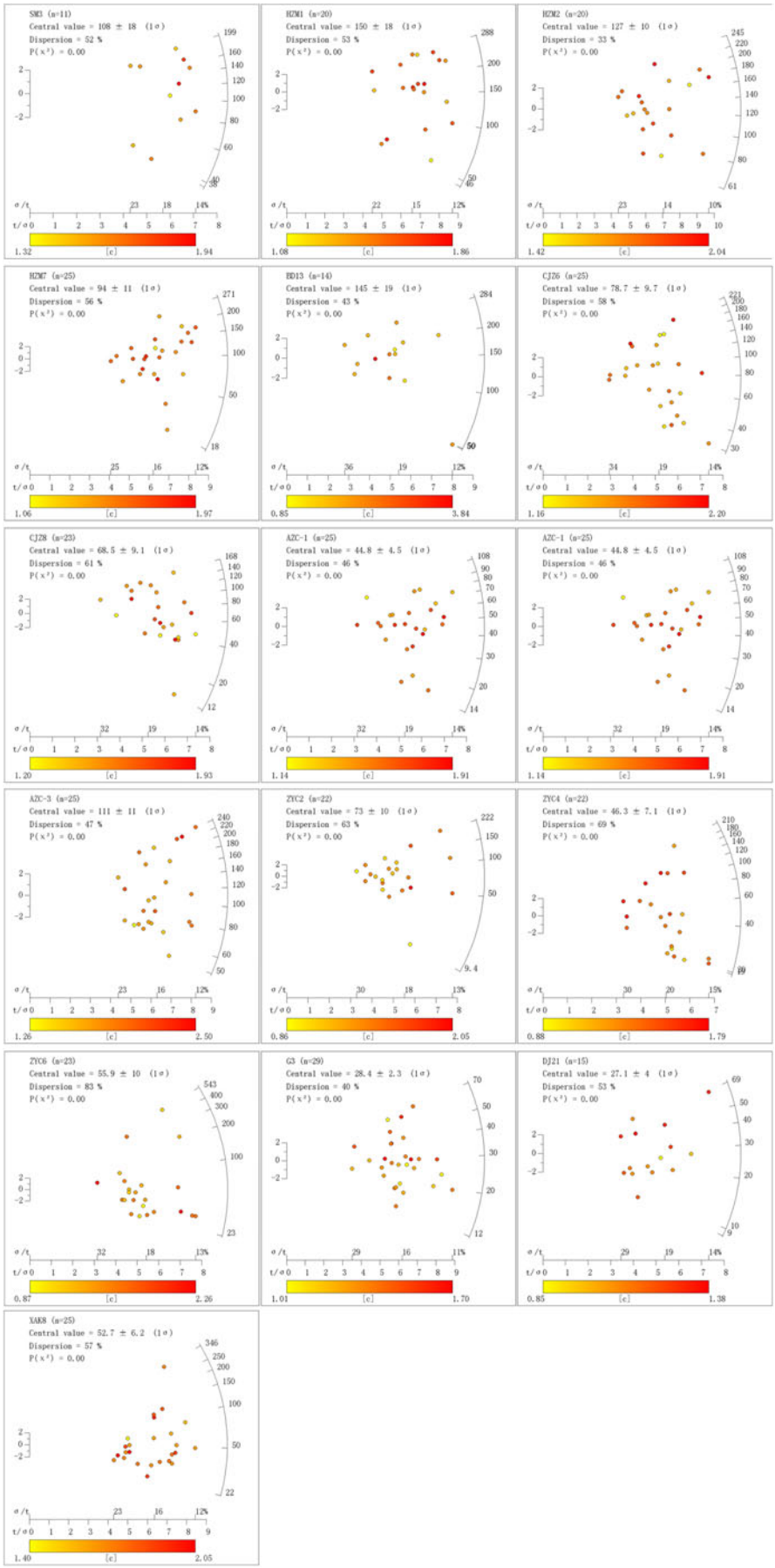

Figure 3. Radial plots of apatite fission track ages of collected samples.

https://doi.org/10.1017/S0016756826100545 Published online by Cambridge University Press

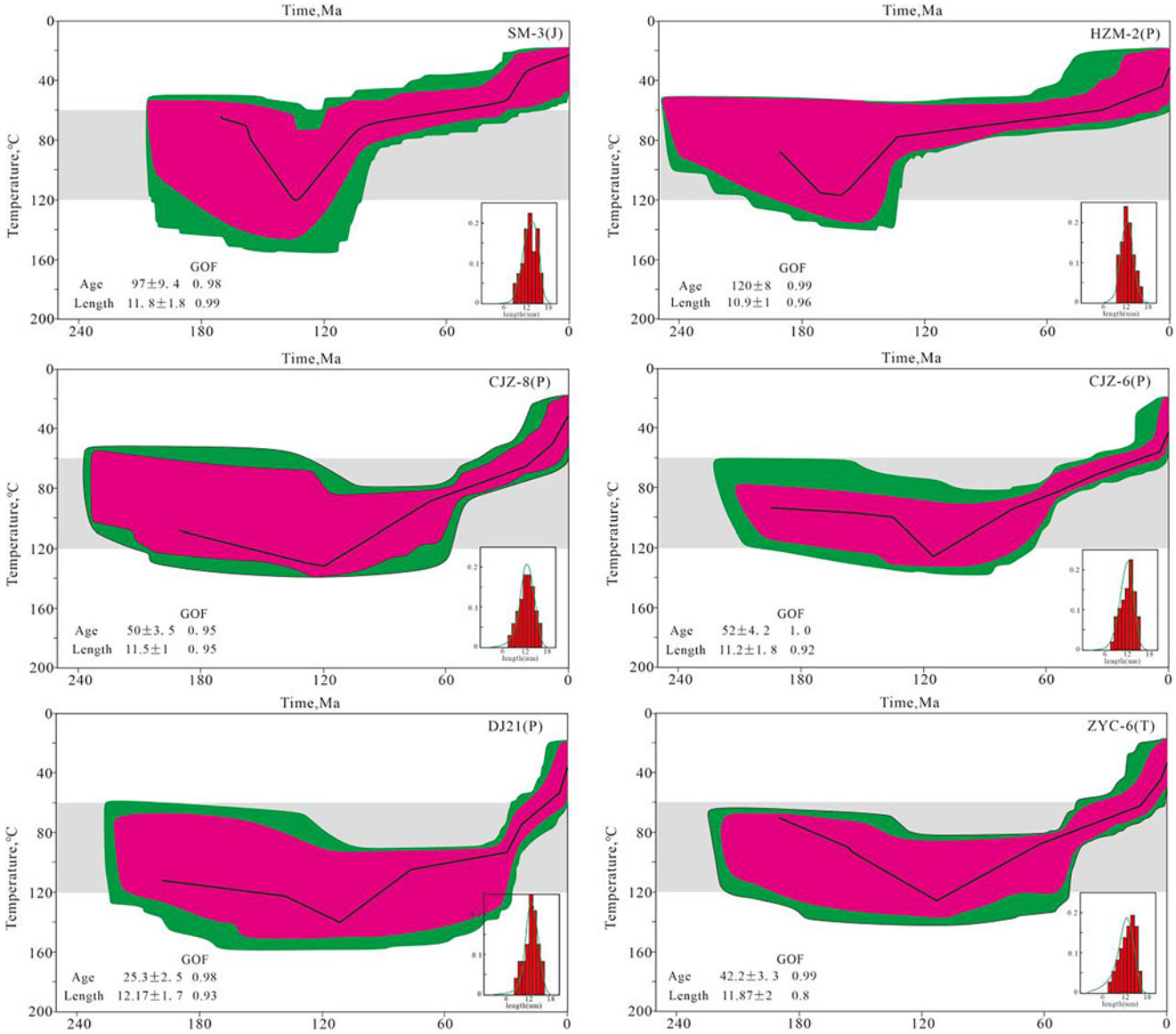

Figure 4. Thermal modelling results showing the time–temperature paths for the Eastern Orods Basin.

above the total annealing temperature (>110°C) and a present-day surface temperature constrained to 0–20°C. The Goodness-of-Fit (GOF) coefficients ranged from 0.8 to 0.99, indicating a good fit for the results.

Within these acceptable fit ranges, the modelling results indicate that each sample recorded two or three significant cooling stages. The cooling rate has progressively decreased since the Early Cretaceous, and there are distinct differences in cooling rates between the northern and southern areas. The envelopes for samples SM-3 and HZM-2 from the northern area reached their maximum burial depth at approximately 140 Ma, exceeding the 120°C isotherm. They began to experience a major cooling event from 140–100 Ma (Late Jurassic–Early Cretaceous), passing through the annealing zone. Similarly, samples D21 and ZYC-6 from the southern area experienced higher temperatures and began rapid uplift at 120 Ma (Early Cretaceous), slightly later than the northern and central areas. Since the Neogene, their temperatures have decreased to below 60°C. Samples CJZ6 and CJZ8, located in the central part of the eastern margin, primarily reflect a rapid cooling stage during the Early Cretaceous (ca. 130–120 Ma).

Despite the dispersion in single-grain ages, the AFT data and the model path provide clear evidence for a multi-stage and spatially heterogeneous exhumation history across the eastern Ordos Basin since the Late Jurassic. The thermal history models, constrained by fully reset samples that once reached temperatures >120°C, consistently reveal a complex three-stage cooling pattern. This pattern is well-exemplified by sample SM-3 from the northern area, which records the following: (1) an initial, major exhumation phase (140–70 Ma) with a cooling rate of ~1.5°C/Ma; (2) a subsequent period of relative tectonic quiescence or slow exhumation (70–30 Ma) at ~0.25°C/Ma; and (3) a final, rapid phase of uplift and cooling that initiated at ~30 Ma, with a cooling rate of ~2°C/Ma. This detailed evolution for the eastern margin contrasts with the thermal history of the central part of the basin, where previous studies of the central basin identified a simpler, two-stage process. This two-stage process involved a prolonged cooling phase from 120–30 Ma (late Early Cretaceous–Palaeogene) at a rate of 2.5°C/

https://doi.org/10.1017/S0016756826100545 Published online by Cambridge University Press

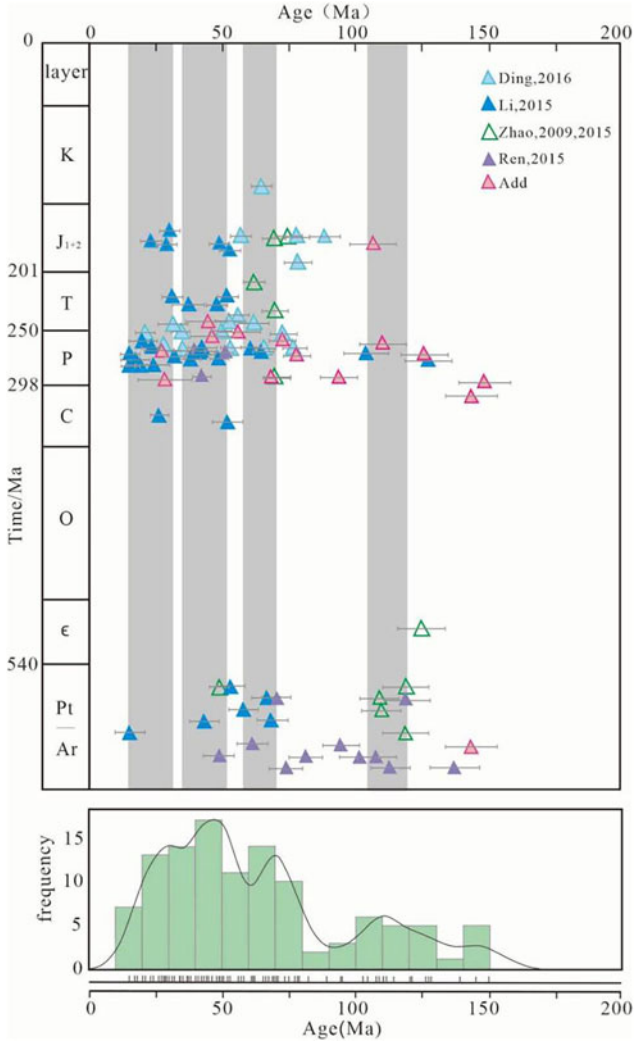

Figure 5. Apatite fission track age distribution maps of eastern Ordos Basin.

Ma, followed by a more rapid cooling phase since 30 Ma (Neogene) at 3.6°C/Ma (Chen *et al.* 2022). This discrepancy confirms that the eastern basin margin underwent non-uniform uplift and cooling along its north-south extent, providing important constraints on the tectonic evolution of the eastern boundary of the Ordos Basin.

The thermal history recorded by these samples begins with a period of post-Triassic burial and heating. This was followed by an initial phase of rapid cooling that commenced at approximately 140–120 Ma. Subsequently, the samples cooled at a slower rate as they passed through the Apatite PAZ (mostly 80°C–120°C), before undergoing a final episode of accelerated cooling since 30 Ma. The weighted average paths of all samples show that they experienced similar cooling stages.

5. Discussion

To better understand the tectono-thermal evolution and regional geodynamic background of the eastern Ordos Basin since the Mesozoic, this study has compiled previously published AFT thermochronology data (Zhao *et al.* 2009; Ren *et al.* 2014; Li *et al.* 2015; Ren *et al.* 2015; Zhao *et al.* 2015; Ding *et al.* 2016; Zhang *et al.* 2021a) (Figure 1). The significant variation observed in the AFT ages and the dispersion noted in the modelling is indicative of a non-uniform tectono-thermal history, with tectonic processes exhibiting pronounced spatial heterogeneity. Furthermore, thermal history modelling of this data reveals multi-stage and asynchronous cooling processes, suggesting that the evolution of the eastern Ordos Basin is the product of multiple, superimposed tectonic regimes.

5.a. Thermochronological analysis

Previous studies indicate significant north-south variation in the magnitude of exhumation across the eastern Ordos Basin. Vitrinite reflectance (Ro) in the eastern Ordos Basin ranges from 0.7% to 3.1% (Figure 1b), with thermal maturity gradually increasing from north to south. In the northern Baode area, values range from 0.6%–0.9%; in the Linxing area, Ro values are concentrated between 0.8% and 1.4%; and in the southern Daji area, they span from 1.3%–3.1%. The erosion thickness, estimated from vitrinite reflectance and sonic log data, is approximately 1500 m in the northern area but increases southward to >2000m (Yu *et al.* 2017; Li *et al.* 2018). The erosion thickness in the south is significantly greater than in the north. Barker (1986) utilized a large dataset of mean vitrinite reflectance (Rm) from humic organic matter and their corresponding maximum temperatures (*T*max) to establish the regression equation:

$$ln(Rm) = 0.0096Tmax - 1.4,$$

This equation is used to estimate the maximum palaeotemperatures experienced by rocks during their geological history. Based on calculations, the Tmax for the Shanxi Formation in the northern Baode area is 115.7°C. In the central Linxing area, Tmax for the Shanxi-Benxi Formations ranges from 142.4–163.3°C, and in the southern Daji area, it ranges from 208.9–239°C. These temperatures exceed the AFT closure temperature. This indicates that the measured AFT ages represent the time when the samples cooled through the AFT PAZ during a later phase of tectonic uplift. Therefore, the AFT ages record the Meso-Cenozoic uplift history.

The AFT ages of almost all detrital grains are older than their stratigraphic ages. This suggests that in certain areas or at certain stratigraphic levels, post-depositional burial was insufficient to heat the samples into the AFT PAZ, or that the samples experienced 120–60°C temperatures for a very short duration. By integrating previously published AFT data, Peng *et al.* (2023) found that the detrital AFT ages are mainly concentrated in four ranges (Figure 5): Peak 1 (120–110 Ma), Peak 2 (70–60 Ma), Peak 3 (50–40 Ma), and Peak 4 (30–20 Ma). The distribution of AFT ages also suggests that the apatite grains may have been derived from multiple source regions. Based on the AFT data from the eastern segments, ages corresponding to Zone 1 and Zone 2 are found mainly in the northern and central areas, whereas ages from Zone 3 and Zone 4 are distributed throughout the eastern area (Figure 6).

The abundance of P1 and P2 age peaks in the northern and central areas indicates that these segments were among the first areas (ca. 120 Ma) to be affected by the destruction of the NCC, with significant early activity along marginal faults. The northern area had greater palaeotopographic relief and a higher exhumation rate, which facilitated the earlier uplift of deep-seated rocks above the AFT closure temperature zone. The P1 and P2 peaks reflect the onset of uplift in the northern and central areas during the early Mesozoic (110–70 Ma). The northern area (P1) cooled earliest at a

https://doi.org/10.1017/S0016756826100545 Published online by Cambridge University Press

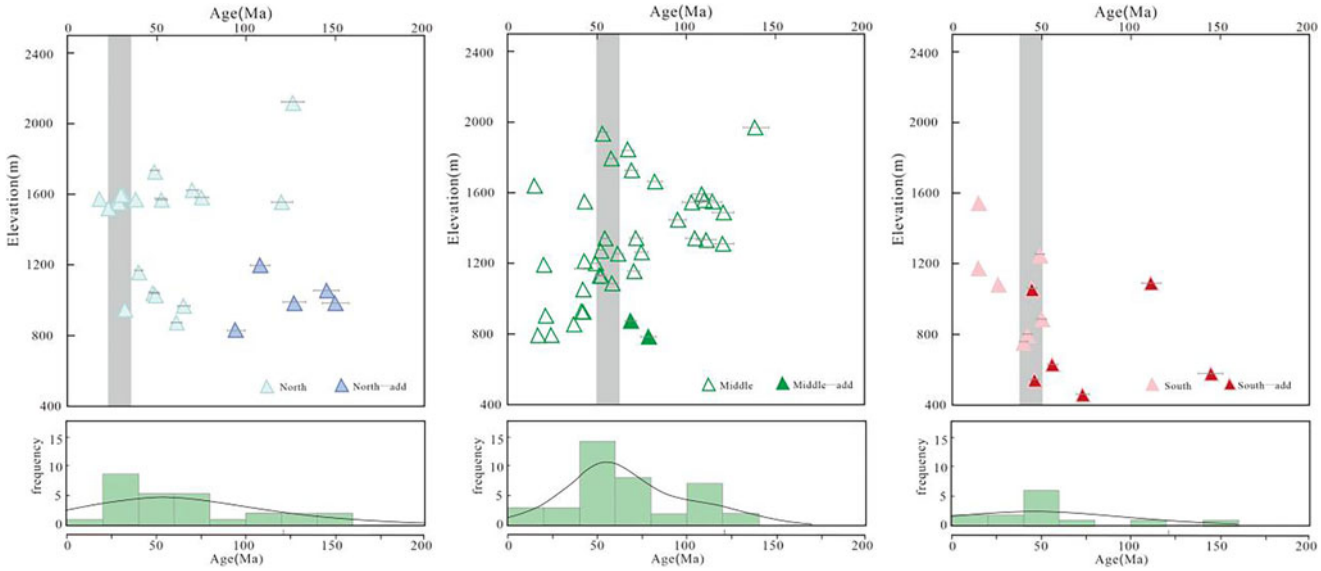

Figure 6. Apatite fission track age distribution maps of the northern, central and southern segments of the eastern Ordos Basin.

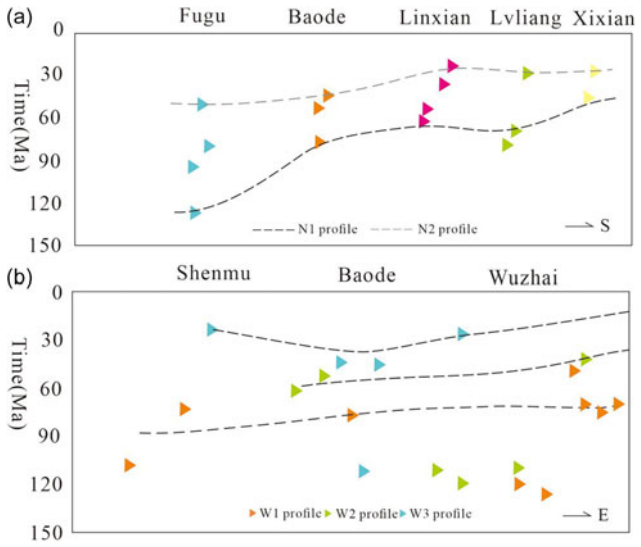

Figure 7. AFT fission track age profiles in eastern Ordos: a) North-South profile and b) West-East profile.

relatively moderate rate represents this 'medium-temperature, medium-speed' cooling. In contrast, the cooling process in the central segment was more continuous, extending to 60–70 Ma, with a moderate cooling rate of approximately 2.5°C/Ma (Chen *et al.* 2022), reflecting the influence of inherited tectonic activity superimposed by Cenozoic far-field uplift. The central area exhibits a 'multi-stage, medium-speed' cooling pattern.

The southern area is dominated by the younger P3 (40–50 Ma) and P4 (20–30 Ma) age peaks, indicating a later onset of major tectonic activity. This area shows no significant cooling signal during the Cretaceous, likely because a thicker sedimentary cover prevented the deep-seated rocks from being exhumed into the AFT PAZ at that time. Instead, this area experienced intense Cenozoic inversion, driven by far-field compressional stresses emanating from the Tibetan Plateau, which significantly enhanced Neogene uplift (Peng *et al.* 2019; Zhang *et al.* 2021a). This later, rapid uplift, resulted in the southern area cooling through the AFT closure temperature during 50–20 Ma, thereby recording the P3 and P4 peaks.

The widespread appearance of P3 and P4 peaks across the entire eastern margin is attributed to tectonic reactivation in the early Cenozoic. The period since 30 Ma, in particular, marks the most intense phase of uplift for the eastern Ordos Basin. Far-field stresses from the ongoing growth of the Tibetan Plateau drove the inversion and strike-slip reactivation of marginal faults, enhancing tectonic activity and causing widespread, significant exhumation and cooling throughout the eastern margin (Huang *et al.* 2021; Zhang *et al.* 2021*a*; Peng *et al.* 2023). This regional trend is clearly illustrated by the AFT ages transect from Fugu in the north to Xixian in the south (Figure 7a). East-west profiles show little variation in AFT ages along the same profile, whereas north-south profiles reveal a distinct trend of younger ages from north to south (Figure 7b). This indicates significant differential cooling and thermal evolution across the region. This north-south age gradient reflects differential tectonic uplift and exhumation since the Mesozoic, with the influence of tectonic activity at the margin of the NCC being particularly pronounced.

Samples in the north record the older P1, P2 and P3 uplift and cooling events, suggesting they captured earlier phases of Mesozoic thermal activity or uplift. In contrast, the southern area is dominated by younger AFT ages, indicating that its exhumation was delayed but more intense, concentrated primarily in the 50–20 Ma period, reflecting significant Palaeogene-Neogene tectonic uplift and rapid cooling. This spatial pattern of cooling ages, which young southward, is intrinsically linked to regional inversion structures, the activity of basin-boundary faults, and tectonic movements at the margin of the NCC.

5.b. Uplift and exhumation history of the eastern Ordos Basin

The eastern Ordos Basin lies within the TNCO, where the NCC, assembled from Archaean-Palaeoproterozoic micro-continental blocks (Zhao *et al.* 2005, 2016; Duan, 2024). The basin exhibits an east-west differentiation, with the Western Block having a lithospheric thickness of 150–200 km and low heat flow values

https://doi.org/10.1017/S0016756826100545 Published online by Cambridge University Press

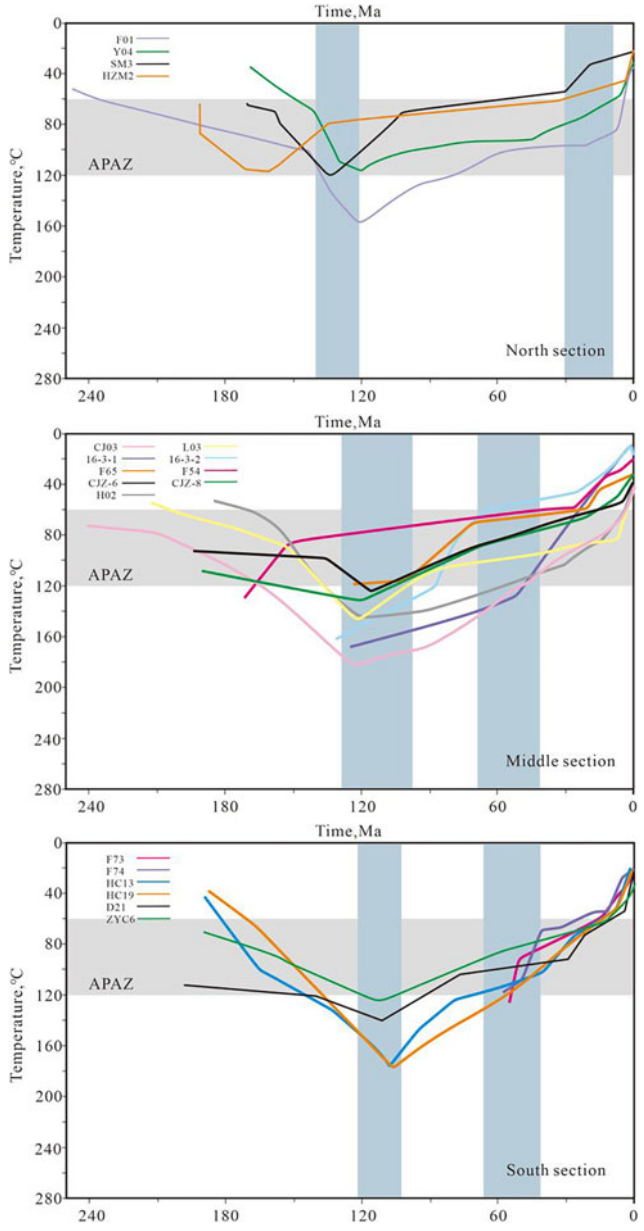

Figure 8. Thermal history modelling results for the northern, middle, and southern sections of the Eastern Ordos. The different coloured lines represent the best-fit paths from different samples. Data are from Ding (2016), Huang (2016), Ren (2015), and Wang (2024) and this study.

(40–60 mW/m^2), preserving typical cratonic attributes (Zhu *et al.* 2015). In contrast, during the Mesozoic, both the TNCO and the Eastern Block underwent a massive lithospheric thinning event, where the lithosphere was reduced to 60–80 km, accompanied by elevated heat flow (>70 mW/m^2). Lithospheric thinning in the Ordos Basin initiated during the latest Jurassic and culminated in the Early Cretaceous. According to reconstruction results (Qi *et al.* 2025), the lithospheric thickness in the eastern basin was reduced to 61 km by the Early Cretaceous. Subsequently, the eastern lithosphere has re-thickened to 81 km since the Cenozoic due to thermal subsidence. Thermal inversion modelling reveals high-temperature anomalies within the TNCO, indicating the upwelling of deep, hot mantle materials (Zhang *et al.* 2025). This lithospheric thinning and mantle thermal activity resulted in a peak heat flow in the eastern basin during the Early Cretaceous. Since the Late Cretaceous, with the waning of tectonic activity, the lithosphere has gradually cooled and re-thickened. Consequently, the thermal regime of the basin has stabilized, ultimately evolving into its present-day "warm basin" status (Qi *et al.* 2025).

It is well-established that the tectono-thermal history of the eastern Ordos Basin region, including the Taihang-Lvliang Mountains, is marked by at least three significant episodes of rapid exhumation since the Mesozoic (Figure 8): in the Late Jurassic (ca. 150 Ma) (Figure 9a), the Late Cretaceous, the Eocene (ca. 50–40 Ma) and the Late Oligocene–Early Miocene (ca. 30–20 Ma) (Huang *et al.* 2021; Zhang *et al.* 2021a). Previous research (Ren *et al.* 2007; Chen *et al.* 2013) has reconstructed palaeotemperatures using multiple methods on Upper Palaeozoic samples, including vitrinite reflectance, fluid inclusions, apatite fission track and illite crystallinity. These authors concluded that the palaeogeothermal gradient along the eastern Ordos Basin during the Late Mesozoic was 2.9–4.0°C/100m. Temperatures reached peak values during the Early Cretaceous, corresponding to a geothermal gradient of 40°C/km, followed by 32°C/km during the Late Cretaceous–Palaeogene and 28°C/km during the Neogene. Exhumation rates were calculated based on these values.

The erosion rate can be estimated using the closure temperature of individual minerals and the fission-track ages of samples, combined with the regional palaeo-geothermal gradient, to calculate the long-term average uplift rate of a sample since it cooled through its closure temperature (Parrish, 1983). The calculation is expressed as: $U = \frac{T_B - T_S}{G \times t}$, where U is the long-term average uplift rate of the sample, m/Ma; T_B is the closure temperature of the mineral, taken as 110°C for apatite and 240°C for zircon; T_S is the mean annual surface temperature of the study area, assumed to be 20°C; G is the palaeo-geothermal gradient of the area, °C/100 m; and t represents the AFT age of the sample, Ma. Through a comparative analysis of the tectono-thermal processes in the northern, central and southern areas of the eastern basin, we conclude that the eastern Ordos Basin has undergone a three-stage tectono-thermal evolution since the Mesozoic. However, the thermal history paths of individual samples show variations in the onset, duration and rate of these three rapid uplift phases, characterizing the uplift process as differential.

5.b.1. Early cretaceous to late cretaceous

The Early Cretaceous was a key turning point in the tectonic history of the Ordos Basin. During this period, the thickened ancient lower crust of the NCC sank into the underlying asthenosphere, driven by the subduction of the Palaeo-Pacific Plate beneath the Eurasian continent (Figure 9b). This deep process triggered the upwelling of the asthenospheric mantle, leading to significant lithospheric thinning and an elevated regional geothermal gradient (Zhang *et al.* 2022). As a direct result of this process, the lithosphere in the central transition zone of the NCC currently has a thickness of 100 to 140 km, and shows significant west-to-east thinning (Ren *et al.* 2002; Zhu *et al.* 2015; Ren *et al.* 2021).

Most of the AFT data record this tectono-thermal event of the Early Cretaceous, which represents the first cooling stage in the east. The modelling results (Figure 4) indicate that the Early Cretaceous was the main uplift period for the eastern region. The region experienced overall uplift, with differential cooling occurring between approximately 130 and 110 Ma. These two cooling phases are clearly reflected in the AFT ages obtained from the

https://doi.org/10.1017/S0016756826100545 Published online by Cambridge University Press

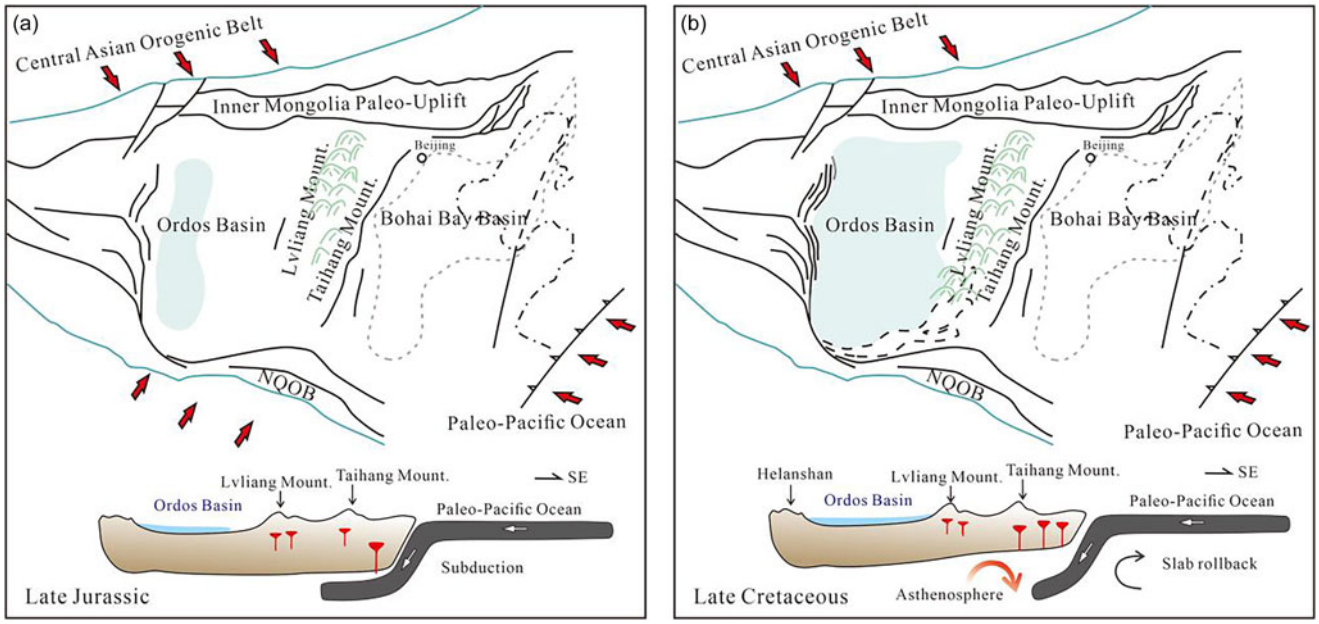

Figure 9. Schematic summary of the mainly Mesozoic–Cenozoic tectonic history of Eastern Ordos and its surroundings (a) Late Jurassic (b) Late Cretaceous with reference to Huang et al. (2021).

eastern part. More specifically, by ca. 130 Ma, strata in the eastern part had subsided to their maximum depth, reaching 120°C in the north and 150°C in the south. During the Early Cretaceous, the entire eastern region began to uplift at relatively low cooling rates, approximately 25 m/Ma in the northern area (sample SM3), 33 m/Ma in the central area (sample CJZ-8), and 50 m/Ma in the southern area (sample ZYC6), indicating that the region experienced a similar overall exhumation process.

A rapid cooling event occurred between 130–100 Ma, marking the key transition of the Ordos Basin from burial heating to uplift and cooling. The onset of uplift was earlier in the north (ca. 130 Ma) compared to the south (ca. 110 Ma). Thermal history modelling (using a geothermal gradient of approximately 40°C/km (Chen *et al.* 2013) shows a temperature decrease of about 20–60°C. This decrease corresponds to an exhumation depth of 0.5–1.5 km, indicating significant tectonic uplift, with the uplift rate in the north being significantly higher than in the south. The magnitude of erosion across the entire basin gradually increases towards the eastern margin and the southeast. Additionally, magmatic intrusions occurred in the Zijinshan area of the central section (136.7–130.4 Ma) (Chen *et al.* 2013). The Zijinshan intrusive rocks are characterized by a deep magma source from the crust-mantle transition zone, indicating lithospheric delamination, extension and asthenospheric upwelling in the central NCC during the Early Cretaceous. This tectono-thermal event led to intensified exhumation in the region, resulting in the differential uplift of the eastern margin since the Early Cretaceous.

5.b.2. Late cretaceous to Palaeogene

The second major exhumation phase in the eastern Ordos Basin occurred between approximately 70 and 40 Ma. This period was governed by a complex interplay of regional tectonic forces. Since the Late Cretaceous, the basin had been in a state of long-term uplift and denudation, driven primarily by the subduction of the Palaeo-Pacific Plate to the east (Ren *et al.* 2015; Suo *et al.* 2012). This resulted in a regional depositional hiatus and transformed the eastern margin into a source area for erosion, with Jurassic and Cretaceous strata becoming widely absent. Based on a geothermal gradient of 32°C/km (Chen *et al.* 2013), this corresponds to a maximum exhumation depth of about 1 km. During this stage, the overall uplift rate of the eastern part of the region slowed down, the exhumation thickness was not substantial, and a process of relatively slow uplift was maintained.

Regionally, the collision between the Indian and Eurasian plates occurred between 60 and 50 Ma, leading to eastward and southeastward extrusion (Zhang *et al.* 2021a). Concurrently, the subduction direction of the Palaeo-Pacific Plate shifted from NNW to NWW between 50 and 42 Ma, causing tectonic inversion in eastern China (Chen *et al.* 2022). During the Late Cretaceous, the study area was characterized by a depositional hiatus and intense exhumation, transforming it into a source area for erosion. Furthermore, the basin and its periphery underwent regional exhumation, and the tectonic stress field shifted to compressional (Figure 10) (Zhang *et al.* 2021a; Shi *et al.* 2019), forming a series of thrust-fold belts and strike-slip structures (Chen *et al.* 2025).

5.b.3. Since the Palaeogene

Since 30 Ma, the lithosphere of the eastern NCC has thinned significantly. The interior of the basin exhibited overall uplift, while a series of graben and pull-apart basins developed along its periphery. The most prominent feature on the eastern margin is the formation and evolution of the Shanxi Graben. Low-temperature thermochronology studies confirm that the Lvliang and Taihang Mountains underwent renewed, albeit slow, uplift and denudation during this time (Ren *et al.* 2015; Zhang *et al.* 2021a; Huang *et al.* 2021; Li & Song 2010). This tectonic framework, which has shaped the modern landscape of North China, is considered a far-field response to the interplay between the ongoing uplift of the Tibetan Plateau and the subduction of the Pacific Plate. The AFT data consistently record this Cenozoic event, with a prominent age peak between 30 and 20 Ma. The acceptable thermal history path indicates that most sample paths passed through the PAZ during this time and show a 'fast-

https://doi.org/10.1017/S0016756826100545 Published online by Cambridge University Press

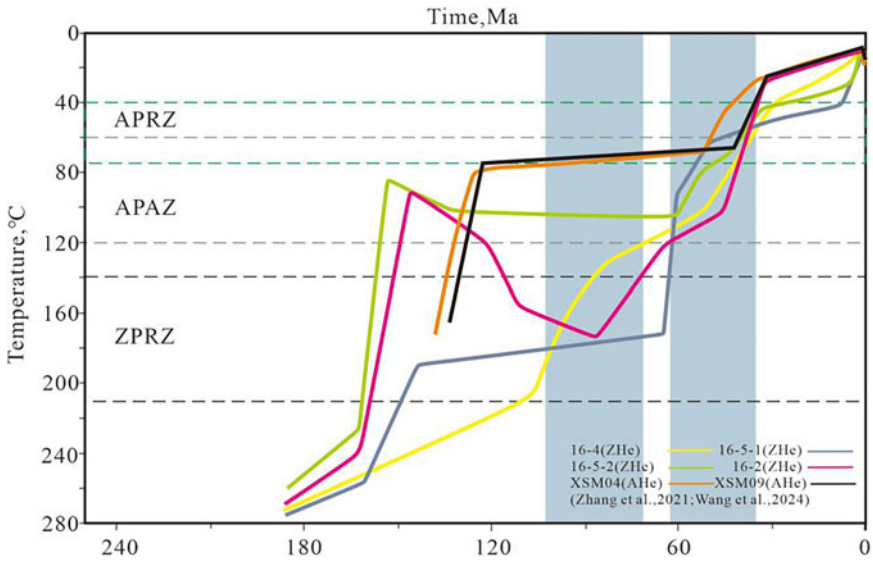

Figure 10. Thermal history modelling results based on other thermochronological methods in the eastern Ordos Basin (simulation results are from Zhang, 2021 and Wang, 2024).

slow-fast' cooling pattern since 30 Ma. Based on a geothermal gradient of 28°C/km (Chen *et al.* 2012), the total Cenozoic exhumation is estimated at 1.8–2.1 km. This Neogene uplift was also differential, with exhumation rates of ~35 m/Ma in the northern (SM3) and central (CJZ-6) areas, increasing to a more rapid ~54 m/Ma in the southern area (D21, HC19). This southward intensification of uplift is consistent with a greater far-field effect from the Tibetan Plateau on the southern part of the basin.

By integrating ZFT/AFT and (U-Th)/He (ZHe/AHe) thermochronometers with varying closure temperatures (Figure 10), the cooling sequence from deep to shallow crustal levels has been reconstructed (Zhao *et al.* 2016; Zhang *et al.* 2021a; Wang *et al.* 2024). The high-closure-temperature zircon systems (ZFT/ZHe) constrain a rapid cooling event during the Middle Jurassic–Early Cretaceous (180–130 Ma), AFT data record the complex thermal history of the Cretaceous (130–65 Ma), specifically capturing the annealing effects induced by anomalous geothermal gradients during Early Cretaceous extension (Zhang *et al.* 2021a), followed by a phase of rapid exhumation. The age discrepancy between the AFT and ZFT results implies a prolonged cooling interval bridging the Early Cretaceous and the Cenozoic. Finally, low-closure-temperature AHe data (Wang *et al.* 2024) record the final cooling stage from shallow depths to the surface, with ages ranging from 41.6 to 80.5 Ma, confirming a regime of slow uplift since the Cenozoic.

In summary, the post-Early Cretaceous evolution of the Ordos Basin can be synthesized into a three-stage history of differential uplift (Figure 11). (1) During the Early Cretaceous, significant uplift was concentrated in the northern and central areas, while the south remained a zone of subsidence or very slow uplift. (2) In the Late Cretaceous–Palaeogene, the basin experienced slight regional uplift, with the southern area beginning to experience slow-to-moderate uplift. (3) During the Neogene, the entire basin entered a phase of accelerated regional uplift, with the southern area exhibiting the highest rates. This complex, diachronous history, driven by the evolving interplay of regional stress fields, has resulted in the removal of up to 2 km of Mesozoic strata from the eastern margin (Yang *et al.* 2024).

Such long-term uplift has exerted a profound influence on petroleum systems. Tectonic uplift since the Late Cretaceous not only slowed organic matter maturation but also destroyed early-formed hydrocarbon reservoirs. While the Permian-Jurassic served as a critical period for burial and thermal maturation, the subsequent uplift and denudation during the Early Cretaceous led to a rapid decrease in temperature. The cooling event halted thermal evolution and terminated gas generation. Notably, the timing of the uplift determined the duration of the hydrocarbon generation window. The northern area of the eastern margin experienced early uplift, resulting in a truncated accumulation period and weaker generation intensity. In contrast, the southern underwent later uplift, allowing source rocks to remain within the hydrocarbon generation window for a longer duration. Furthermore, the uplift from the Late Cretaceous to the Neogene disrupted the original preservation conditions, leading to a decline in formation pressure and the dissipation of natural gas. This process directly resulted in the low-pressure characteristics observed in present-day reservoirs; specifically, the northern region developed into undersaturated, low-pressure coalbed methane reservoirs due to tectonic uplift and modification (Tao *et al.* 2018).

As a major, stable block in China, the eastern Ordos Basin has recorded a complex history of uplift and cooling in response to regional tectonic events, which have driven both basin-wide and differential uplift (Figure 11). Its evolution since the Mesozoic has been primarily governed by the interplay between tectonic activity and lithospheric thermal processes. Situated in a transitional zone between the craton and an active orogenic belt, the study area is dissected by a series of large-scale fault systems. These faults have experienced repeated reactivation since the Mesozoic, triggering intense crustal uplift, which in turn led to rapid surface denudation and rock cooling. This process was further exacerbated by thermal anomalies associated with lithospheric thinning. Ultimately, the complex thermal history of the eastern Ordos Basin was sculpted by the coupling of these surface processes – uplift, exhumation and cooling – with deep mantle dynamics.

To contextualize the thermal evolution of the eastern Ordos Basin within a global framework, a comparative analysis was conducted with the Beaufort-Mackenzie Basin (BMB) in Canada and the Eastern Brazilian Margin Basins. The BMB, a typical continental margin foreland basin, experienced significant Cenozoic tectonic activity associated with the Cordilleran and Eurekan orogenies, leading to multiple phases of tectonic uplift and exhumation (Midwinter *et al.* 2017). Despite differing tectonic settings – BMB as a foreland basin and the Ordos Basin as a stable cratonic basin – both regions underwent pronounced tectonothermal events during the Late Cretaceous to Palaeogene, which are clearly recorded by AFT data (Midwinter *et al.* 2017). The thermal history of the BMB is

https://doi.org/10.1017/S0016756826100545 Published online by Cambridge University Press

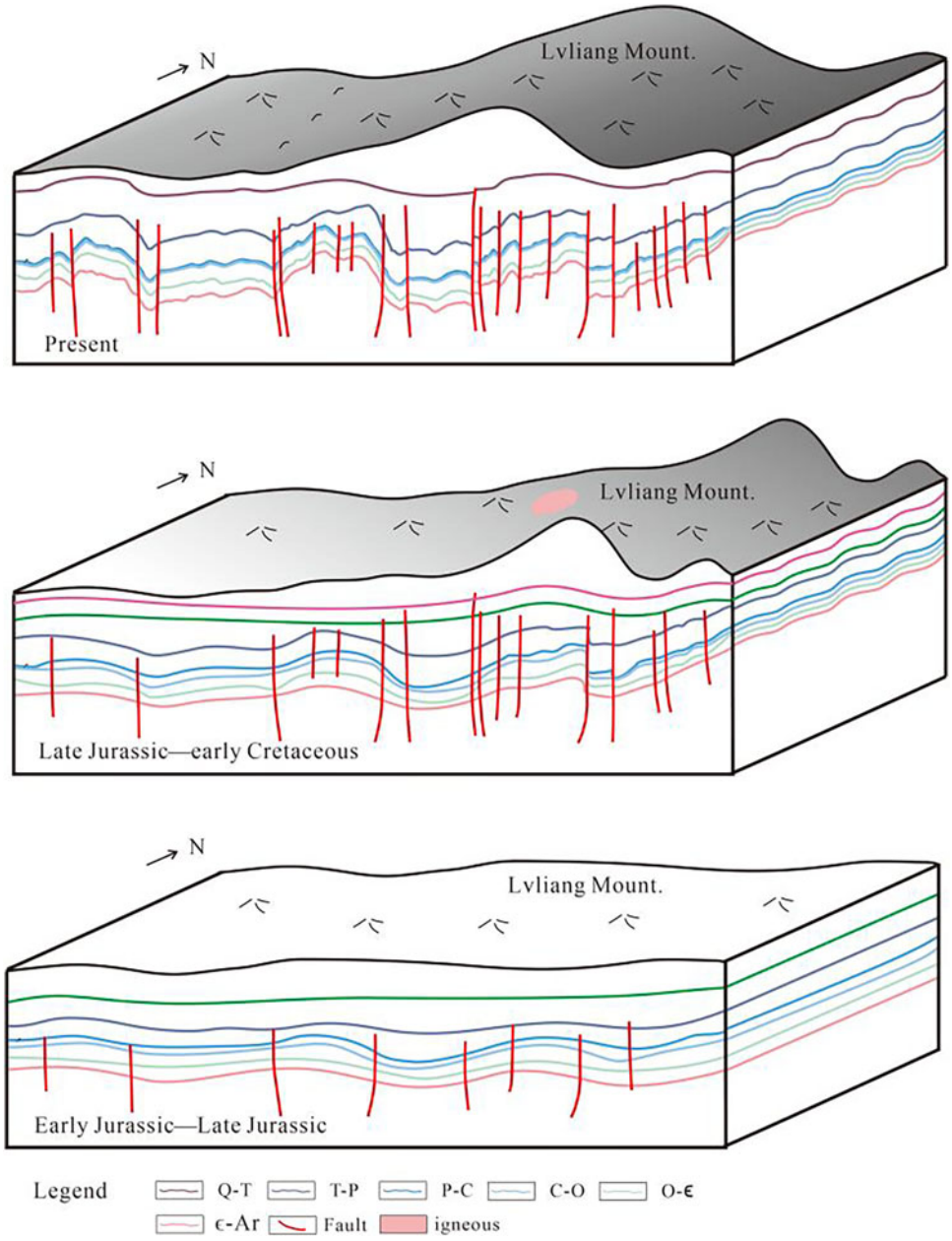

Figure 11. Evolutionary model of a profile through the Eastern Ordos Basin since the Mesozoic.

primarily burial-driven, governed by the accumulation of thick Cenozoic sediments (over 12–16 km), which significantly contributed to subsurface heating (Tang *et al.* 1992). In contrast, the thermal evolution of the eastern Ordos Basin during the Early Cretaceous was marked by a high heat flow regime, closely related to the lithospheric thinning and extension of the NCC (Ren *et al.* 2020), as evidenced by thermal modelling and AFT analyses. Meanwhile, the Eastern BMB underwent an intense tectonothermal event in the Early Cretaceous, interpreted as the consequence of lithospheric rupture, mantle upwelling and continental rifting. This event resulted in elevated palaeotemperatures (Fonseca *et al.* 2022; Cogné *et al.* 2011). AFT thermochronology effectively captured both this heating phase and the subsequent Cenozoic cooling and uplift, demonstrating the prolonged thermal and tectonic evolution of these passive margins well beyond the rifting phase (Costa *et al.* 2024).

6. Conclusions

(1) The eastern Ordos comprises four AFT (Apatite Fission Track) age zones: P1 (110 Ma), P2 (70 Ma), P3 (50 Ma) and P4 (30 Ma). These zones exhibit spatial variations: the Early Cretaceous (P1) and Late Cretaceous (P2) age peaks are predominantly concentrated in the northern and central areas, indicating that these areas initiated tectonic uplift and exhumation/cooling in the early stages of the NCC destruction, with the northern area cooling earliest. In contrast, the Eocene (P3) and early Miocene (P4) age peaks are widely distributed across the entire eastern margin, with the southern area showing the highest concentration. The later cooling time in the southern area reflects the intense characteristics of Neogene tectonic activity.

https://doi.org/10.1017/S0016756826100545 Published online by Cambridge University Press

(2) Since the Mesozoic, the Ordos Basin experienced three phases of uplift. In the Early Cretaceous, the northern and central areas generally underwent uplift, with rates around 25 m/Ma. Uplift in the southern area initiated slightly later, but its rate of approximately 50 m/Ma was higher than that further north. The region experienced similar denudation processes but exhibits clear north-south differences. During the Late Cretaceous–Palaeogene, overall uplift activity in the basin was relatively low. Since the Neogene, the southern uplift rate has been significantly high, at approximately 54 m/Ma, while the northern and central regions also showed higher uplift rates, around 35 m/Ma. This may be related to the far-field effects of the Qinghai-Tibet Plateau uplift, which imposed a stronger driving force on the southern area of the basin. The complex interplay of regional tectonic stress field evolution and thermal history led to differential tectonic uplift and subsidence processes in the northern, central and southern areas across various geological periods.

(3) Since the Mesozoic, uplift and cooling processes in the eastern Ordos Basin have been primarily controlled by tectonic activity and lithospheric thermal evolution. The region has undergone intense and repeated faulting and crustal uplift, leading to rapid surface exhumation and rock cooling. Furthermore, thermal anomalies resulting from lithospheric thinning have intensified this process. Therefore, the tectonic uplift–exhumation–cooling processes in the eastern basin are coupled with deep mantle processes, jointly shaping the complex thermal evolution history of the eastern Ordos Basin. Early-stage stratigraphic uplift may impede the thermal maturation of source rocks, while late-stage uplift can promote natural gas leakage and dissipation.

Acknowledgements. This study is supported by The PetroChina Changqing Oilfield Company Science and Technology Major Project 'Research on Tectonic-Sedimentary Environment, Hydrocarbon Accumulation Conditions and Favorable Exploration Zones in the Deep Strata of Ordos Basin' (2024D1JC06), and Petrochina Coalbed Methane Company Limited (NCCBM24035KT03). The authors sincerely thank the anonymous reviewers and the editors for their constructive comments and suggestions, which greatly improved the quality of this manuscript.

References

Barker C and Pawlewicz M (1986) The correlation of vitrinite reflectance with maximum temperature in humic organic matter. In *Lecture Notes in Earth Sciences* (eds G Buntebarth and L Stegena), pp. 79–93, Vol. 5. Paleothermics, Springer-Verlag. https://doi.org/10.1007/BFB0012103

Chen G, Deng C, Xu L-M, Zhang H-R, Hu Y-X, Yu F, Li N, Meng X-N and Liu Y (2013) Analysis on the thermal history and uplift process of Zijinshan intrusive complex in the eastern Ordos Basin. *Chinese Journal of Geophysics* **56**(1), 78–90. https://doi.org/10.1002/cjg2.20007

Chen G, Liu C, Jepsen KL, Li W, Zhang J and Wang P (2022) Tectono-thermal events and their constraints on sandstone-type uranium mineralization in the northern Ordos Basin. *Acta Petrologica Sinica* **38**(10), 3123–3144. (in Chinese with English abstract).

Chen G, Sun J, Zhou L, Zhang H, Li X and Wang Z (2007) Fission-track-age records of the Mesozoic tectonic-events in the southwest margin of the Ordos Basin, China. *Science in China Series D: Earth Sciences* **50**(S1), 133–143. https://doi.org/10.1007/s11430-007-6025-y

Chen Y, Li J, Chen L, Zhao H (2025) Mesozoic multi-direction collision tectonic evolution of the Ordos Basin, China: insights from the detrital zircon and apatite (U-Th)/He analyses. *China Geology* **8**(1), 141–158. https://doi.org/10.31035/cg20230068

Clinkscales C, Karlstrom K, Heizler M and Crossey L (2021) Regional exhumation and tectonic history of the Shanxi Rift and Taihangshan, North China. *Tectonics* **40**(3), e2020TC006240. https://doi.org/10.1029/2020TC006416

Cogné N, Gallagher K and Cobbold PR (2011) Post-rift reactivation of the onshore margin of southeast Brazil: evidence from apatite (U-Th)/He and fission-track data. *Earth and Planetary Science Letters* **309**(1–2), 118–130. https://doi.org/10.1016/j.epsl.2011.06.025

Costa DFG, Fonseca A and De Grave J (2024) Relating differential crustal architecture to passive margin evolution: a case study from the Colatina Fracture Zone (SE Brazil) using apatite fission-track thermochronology. *Geological Journal* **59**(10), 2789–2802. https://doi.org/10.1002/gj.5027

Ding C, Chen G, Guo L, Zhang W, Shi X, Xu X and Liu T (2016) Differential uplift on the northeast margin of Ordos Basin: evidence from apatite fission track analysis. *Geology in China* **43**(4), 1238–1247. (in Chinese with English abstract). https://doi.org/10.12029/gc20160410

Donelick RA, O'Sullivan PB and Ketcham RA (2005) Apatite fission-track analysis. *Reviews in Mineralogy and Geochemistry* **58**(1), 49–94. https://doi.org/10.2138/rmg.2005.58.3

Duan Q, Zhai M, Zhu X, Zhou Y and Fan Y (2024) The significance of Mesozoic basement uplift for interpreting the NCC's Precambrian tectonic regime: evidence from the Paleoproterozoic magmatic rocks along the eastern margin of the Lishi Fault. *Precambrian Research* **420**, 107737. https://doi.org/10.1016/j.precamres.2025.107737

Fonseca A, Cruz S, Novo T, He Z and De Grave J (2022) Contrasting exhumation of cratonic and non-cratonic lithosphere revealed by apatite fission-track thermochronology along the edge of the São Francisco craton, eastern Brazil. *Scientific Reports* **12**, 2728. https://doi.org/10.1038/s41598-022-06419-w

Geng Y, Wang X and Shen Q (2000) The age of the Lüliang group in the Lüliang mountains area. *Acta Petrologica Sinica* **16**(2), 199–205. (in Chinese with English abstract).

Gleadow AJW, Duddy IR, Green PF and Lovering JF (1986) Confined fission track lengths in apatite: a diagnostic tool for thermal history analysis. *Contributions to Mineralogy and Petrology* **94**(4), 405–415. https://doi.org/10.1007/BF00376334

Hasebe N, Tamura A and Arai S (2013) Zeta equivalent fission-track dating using LA-ICP-MS and examples with simultaneous U–Pb dating. *Island Arc* **22**(3), 283–299. https://doi.org/10.1111/iar.12040

He X, Liu C, Wang J, Du F and Xiong L (2023) Structural characteristics of the Yushuwan fault in the northeastern Ordos Basin: implications for basin tectonics and hydrocarbon exploration. *Energy Exploration & Exploitation* **42**(3), 1077–1097. https://doi.org/10.1177/01445987231221592

Huang X, Wang Y, Zhang J and Yang Y (2021) Low-temperature thermochronological insights into the Mesozoic–Cenozoic exhumation history of the Taihang–Lvliangshan region: a review. *Geological Journal* **57**(4), 1511–1529. https://doi.org/10.1002/gj.4352

Huang Z, Ren Z and Gao L (2016) Evidence from detrital zircon and apatite fission track for tectonic evolution since cretaceous in southeastern margin of Ordos Basin. *Chinese Journal of Geophysics* **59**(10), 3753–3764. (in Chinese with English abstract). https://doi.org/10.6038/cjg20161020

Ju Y, Wang W, Ren Z, Yang Z, Liu K, Hou B and Xiao L (2025) Multi-stage evolution of the Ordos Basin: its coupled basin-mountain systems and energy resources. *Science China Earth Sciences* **68**(8), 2426–2473. https://doi.org/10.1007/s11430-025-1627-1

Ketcham RA (2005) Forward and inverse modeling of low-temperature thermochronology data. *Reviews in Mineralogy and Geochemistry* **58**(1), 275–314. https://doi.org/10.2138/rmg.2005.58.11

Ketcham RA, Carter A, Donelick RA, Barbarand J and Hurford AJ (2007) Improved modeling of fission-track annealing in apatite. *American Mineralogist* **92**(5–6), 799–810. https://doi.org/10.2138/am.2007.2281

Ketcham, RA, Donelick RA and Carlson WD (1999) Variability of apatite fission-track annealing kinetics: III. Extrapolation to geological time scales. *American Mineralogist* **84**(9), 1235–1255. https://doi.org/10.2138/am-1999-0903

Li J, Liu C, Yue L and Wang J (2015) Apatite fission track evidence for the Cenozoic uplift of the Lvliang mountains and a discussion on the uplift mechanism. *Geology in China* **42**(4), 960–972. (in Chinese with English abstract).

Li J, Yue L, Liu C, Wang X and Li G (2013) The tectonic-sedimentary evolution of the Lvliang mountains since the Miocene. *Journal of Stratigraphy* **37**(1), 93–100. (in Chinese with English abstract).

Li J, Zhang H, Zhao L, *et al.* (2021) Crustal anisotropy beneath the trans-north China orogen and its adjacent areas from receiver functions. *Frontiers in Earth Science* **9**, 753612. https://doi.org/10.3389/feart.2021.753612

Li L (2018) Hydrocarbon generation-expulsion history of Upper Paleozoic source rocks and gas accumulation episodes in the Linxing Block, Ordos Basin [Master's thesis, China University of Petroleum]. China National Knowledge Infrastructure. https://kns.cnki.net/KCMS/detail/detail.aspx?dbname=CMFD202001&filename=1019926947.nh

Li X and Song Y (2010) Cretaceous-cenozoic exhumation history of the Lüliang mountains, north China craton: constraint from fission-track thermochronology. *Journal of Asian Earth Sciences* **84**(2), 296–305. https://doi.org/10.1111/j.1755-6724.2010.00145.x

McDowell FW, McIntosh WC and Farley KA (2005) A precise 40Ar–39Ar reference age for the Durango apatite (U–Th)/He and fission-track dating standard. *Chemical Geology* **214**(3–4), 249–263. https://doi.org/10.1016/j.chemgeo.2004.10.002

Midwinter D, Powell J and Schneider DA (2017) Investigating the paleozoic–mesozoic low-temperature thermal history of the southwestern Canadian arctic: insights from (U–Th)/He thermochronology. *Canadian Journal of Earth Sciences* **54**(9), 1021–1041. https://doi.org/10.1139/cjes-2016-0088

Parrish RR (1983) Cenozoic thermal evolution and tectonics of the coast mountains of British Columbia:1. Fission track dating, apparent uplift rates, and patterns of uplift. *Tectonics* **2**(6), 601–631. https://doi.org/10.1029/TC002i006p00601

Peng H, Wang J, Liu C, Ma M, Ma Q, Li K, Pan J, Li J, Qin Y, Xie Q and Zattin M (2022) Meso-Cenozoic growth of the eastern Qilian Shan, northeastern Tibetan Plateau margin: insight from borehole apatite fission-track thermochronology in the Xiji Basin. *Marine and Petroleum Geology* **143**, 105798. https://doi.org/10.1016/j.marpetgeo.2022.105798

Peng H, Wang J, Liu C, Zhang S and Zattin M (2019) Thermochronological constraints on the Meso-Cenozoic tectonic evolution of the Haiyuan-Liupanshan region, northeastern Tibetan Plateau. *Journal of Asian Earth Sciences* **183**, 103966. https://doi.org/10.1016/j.jseaes.2019.103966

Peng H, Wang J, Liu C, Zhao H, Huang L, Zhao X, Zhang S, Liang C, Wang Z, Cattò S, Jiao X, Zhang L, Zhang T, Zhang D and Zattin M (2023) Long-term and multiple stage exhumation of the Ordos Basin, western North China Craton: insights from seismic reflection, borehole and geochronological data. *Earth-Science Reviews* **238**, 104349. https://doi.org/10.1016/j.earscirev.2023.104349

Qi K, Ren Z, Cui J, Yu Q, Bai F, Liu X, Chen Z and Xing G (2025) Present-day deep geothermal field and lithospheric thermal structure in the Ordos Basin. *Geothermics* **125**, 103198. https://doi.org/10.1016/j.geothermics.2024.103198

Ren J, Tamaki K, Li S and Jun X (2002) Late Mesozoic and Cenozoic rifting and its dynamic setting in Eastern China. *Tectonophysics* **344**(3–4), 175–205. https://doi.org/10.1016/S0040-1951(01)00271-2

Ren X, Zhu W, Zhu X, Wang X and Luo M (2015) Mesozoic-cenozoic uplift-exhumation history in Lvliangshan area of Shanxi: evidences from apatite fission track. *Journal of Earth Sciences and Environment* **37**(1), 63–73. (in Chinese with English abstract).

Ren Z, Cui J, Qi K, Yang P, Liu X, Zhang C, Yang G, Gao Y, Zhang Y and Xing G (2022) New progress in the study of theories and methods for the restoration of thermal evolution history in deep and ultra-deep superimposed basins. *Journal of Northwest University (Natural Science Edition)* **52**(6), 910–929. https://doi.org/10.16152/j.cnki.xdxbzr.2022-06-002

Ren Z, Li W, Liang Y, Wu X, Yu Q, Ren L and Wang W (2014) Tight oil reservoir formation conditions and main controlling factors of Yanchang Formation in southeastern Ordos Basin. *Oil & Gas Geology* **35**(2), 190–198. (in Chinese with English abstract).

Ren Z, Qi K, Li J, Huo X, Cui J, Yang P, Wang K, Wang K, Chen Z and Yang G (2021) Thermodynamic evolution and hydrocarbon accumulation in the Ordos Basin. *Oil & Gas Geology* **42**(5), 1030–1042. (in Chinese with English abstract). https://doi.org/10.11743/ogg20210508

Ren ZL, Qi K, Liu RC, *et al.* (2020) Tectonic-thermal event in the Early Cretaceous of the Ordos Basin: dynamic background and its control on the accumulation period of oil and gas and other mineral resources. *Acta Petrologica Sinica* **36**(4), 1213–1234. (in Chinese with English abstract). https://doi.org/10.11743/ogg20210502

Ren ZL, Zhang S, Gao SL, Cui JP, Xiao YY and Xiao HW (2007) Thermal history of the Ordos Basin and its relation to oil and gas accumulation. *Oil & Gas Geology* **28**(4), 492–499.

Shi G, Soares CJ, Shen C, Wang H, Yang C, Liang C and Liu M (2019) Combined detrital zircon fission track and U-Pb dating of the Late Paleozoic to Early Mesozoic sandstones in the Helanshan, western Ordos fold-thrust belt: constraints for provenance and exhumation history. *Journal of Geodynamics* **130**, 57–71. https://doi.org/10.1016/j.jog.2019.07.001

Suo Y, Li S, Li X, Yu S and Liu B (2012) Cenozoic tectonic evolution of the East Asian continental margin: a review. *Geological Journal* **28**(8), 2602–2618. (in Chinese with English abstract)

Tang J and Lerche I (1992) Analysis of the Beaufort-Mackenzie Basin, Canada: burial, thermal and hydrocarbon histories. *Marine and Petroleum Geology* **9**(5), 510–526. https://doi.org/10.1016/0264-8172(92)90063-K

Tao C, Wang Y, Ni X and Wu X (2018) Key accumulation period for coal-series gas reservoir in upper carboniferous Benxi formation, Linxing block, eastern Ordos Basin. *Journal of China University of Mining & Technology* **47**(3), 531–537. (in Chinese with English abstract).

Vermeesch P (2008) RadialPlotter: a Java application for fission track, luminescence and other radial plots. *Radiation Measurements* **44**(4), 409–410. https://doi.org/10.1016/j.radmeas.2009.05.003

Wang Y, He Z, Bian K, Zhao C, Chen L, Dong R, Zhang J, Zhu Z and Liu G (2024) Tectonic controls on ore deposit exhumation and preservation: a case study of the Handan-Xingtai iron-skarn district. *Geoscience Frontiers* **15**, 101924. https://doi.org/10.1016/j.gsf.2024.101924

Xu Y and He D (2022) Triassic provenance shifts and tectonic evolution of southeast Ordos Basin, Central China. *Palaeogeography, Palaeoclimatology, Palaeoecology* **598**, 111002. https://doi.org/10.1016/j.palaeo.2022.111002

Yang P, Ren Z, Tian T, Cui J, Liu C and Wu H (2023) Tectono-thermal evolution and its relationship with petroleum generation in the Chuxiong Basin, southeastern Tibetan Plateau. *Chinese Journal of Geophysics* **66**(12), 5057–5073. (in Chinese with English abstract). https://doi.org/10.6038/cjg2023Q0927

Yang P, Ren ZL, Fu JH, Bao HP, Xiao H, Shi Z, Wang K, Zhang Y-Y, Liu W-H and Li W-H (2024) A tectono-thermal perspective on the petroleum generation, accumulation and preservation in the southern Ordos Basin, North China. *Petroleum Science* **21**(3), 1459–1473. https://doi.org/10.1016/j.petsci.2023.12.006

Yu Q, Ren Z, Li R, Wang B, Qin X and Tao N (2017) Paleogeotemperature and maturity evolutionary history of the source rocks in the ordos basin. *Geological Journal* **52**(S1), 97–118. https://doi.org/10.1002/gj.3069

Zhang H, Zhao L, Li J, *et al.* (2022) Seismic tomography of the Trans-North China Orogen and its dynamic implications. *Frontiers in Earth Science* **10**, 948040. https://doi.org/10.3389/feart.2022.948040

Zhang J, Wang Y, Qu J, Zhang B, Zhao H, Yun L, Li T, Niu P, Nie F, Hui J and Zhang Y (2021b) Mesozoic intracontinental deformation of the Alxa block in the middle part of central Asian Orogenic belt: a review. *International Geology Review* **63**(12), 1490–1520. https://doi.org/10.1080/00206814.2020.1783583

Zhang J, Wang Y, Zhang B, Zhang B and Zhang Y (2021a) Tectonothermal events in the central North China Craton since the Mesozoic and their tectonic implications: constraints from low-temperature thermochronology. *Tectonophysics* **804**, 228769. https://doi.org/10.1016/j.tecto.2021.228769.

Zhao GC, Sun M, Wilde SA and Li SZ (2005) Late Archean to Paleoproterozoic evolution of the North China Craton: key issues revisited. *Precambrian Research* **136**(2), 177–202. https://doi.org/10.1016/j.precamres.2004.10.002

Zhao J, Liu C, Lu J, Cao J, Yang Y and Xue R (2015) Timing of uplift and evolution of the Lüliang Mountains, North China Craton. *Science China Earth Sciences* **59**(1), 58–69. https://doi.org/10.1007/s11430-015-5153-z

Zhao J, Liu C and Wang X (2009) Uplifting and evolution characteristics in the Lüliang Mountain and its adjacent area during the Meso-Cenozoic. Geological *Review* **55**, 663–672.

Zhu R, Fan H, Li J, Meng Q, Li S and Zeng Q (2015) Decratonic gold deposits. *Science China Earth Sciences* **58**(8), 1523–1537. https://doi.org/10.1007/s11430-015-5139-x

https://doi.org/10.1017/S0016756826100545 Published online by Cambridge University Press